JOURNAL OF GEOPHYSICAL RESEARCH, VOL. 103, NO. A12, PAGES 29,445–29,454, DECEMBER 1, 1998

The effect of field-aligned density variations on time-dependent MHD wave coupling in the magnetotail

Andrew N. Wright

Mathematical Institute, University of St. Andrews, Fife, Scotland

W. Allan

National Institute of Water and Atmospheric Research, Wellington, New Zealand

Abstract. We investigate linear MHD wave mode coupling in the cold plasma limit when the equilibrium density (ρ) varies along the equilibrium magnetic field ($\mathbf{B}$). Our numerical simulations indicate that efficient fast/Alfvén mode coupling persists even when $(\mathbf{B}\cdot\nabla)\rho \neq 0$. The time-dependent picture we develop asymptotes to a normal mode for large t and also recovers the $(\mathbf{B}\cdot\nabla)\rho = 0$ singularity qualitatively. When applied to waves in the magnetotail, we find that Alfvénic disturbances will have an extended structure across the magnetic field and that Alfvén wave packets should be excited on plasma sheet boundary layer (PSBL) or mantle field lines. Alfvén waves driven on PSBL field lines are probably the most observable signature at Earth of wave coupling in the distant tail.

1. Introduction

The large-scale reconfiguration of the geomagnetic tail during flux loading or substorms is described naturally in terms of propagating MHD waves. Since the tail is nonuniform the different MHD waves will couple to one another, and this is likely to be important in regions where the Alfvén speed has a significant gradient such as the plasma sheet boundary layer (PSBL) or the plasma mantle.

Although fast mode waves have been observed in the tail lobe by *Elphinstone et al.* [1995], it is far easier to observe Alfvén waves owing to their guided nature and associated lack of attenuation. Indeed, Alfvén waves that are incident upon the ionosphere produce clear signatures in the F region drift velocity in radar data [e.g., *Walker et al.*, 1992] and ground-based magnetometer chains [e.g., *Ziesolleck and McDiarmid*, 1994], and also optical auroral emissions [*Samson et al.*, 1992].

There is general agreement that efficient fast and Alfvén wave coupling may take place in an equilibrium for which $(\mathbf{B}\cdot\nabla)\rho = 0$. Of course, a real tail equilibrium will never satisfy this condition, and is it important to address the more realistic situation where $(\mathbf{B}\cdot\nabla)\rho \neq 0$. Few studies have considered this situation [*Hansen and Harrold*, 1994; *Schwartz and Bel*, 1984; *Wright and Garman*, 1998], and they present conflicting results. Evidently, this issue requires more investigation and clarification, and this is the principal motivation for the present calculation. It is clearly of great importance to understand the coupling of waves in the $(\mathbf{B}\cdot\nabla)\rho \neq 0$ limit since coupling is most likely to occur in the nonuniform mantle or plasma sheet boundary layer. Even a simple local one-dimensional model of these regions which assumes (in GSM coordinates) $\rho(z)$ and a constant field strength must admit the possibility that the field is not entirely in the x direction, but may have some, albeit small, z component (see Figure 1).

Recently, attention has focused upon Alfvén waves originating from the PSBL and mantle. *A. Wright et al.* (Phasemixing and phase motion of Alfvén waves on tail-like and dipole-like magnetic field lines, submitted to *Journal of Geophysical Research*, 1998; hereinafter referred to as submitted manuscript) present observations of optical emissions which are thought to occur on field lines mapping to the PSBL. The auroral emissions show a phase motion (equatorward) that is opposite to that observed on closed field lines. They suggest that details of wave coupling are different on closed and (effectively open) PSBL field lines and that this can explain the reversal of auroral phase motion. Clearly, the details of Alfvén wave excitation in the magnetotail must be understood, as this provides a powerful method for investigating the equilibrium structure of the tail and wave sources within it. These investigations will also lead to a more complete understanding of data sets associated with the tail.

Paper number 98JA01993.
0148-0227/98/98JA-01993$09.00

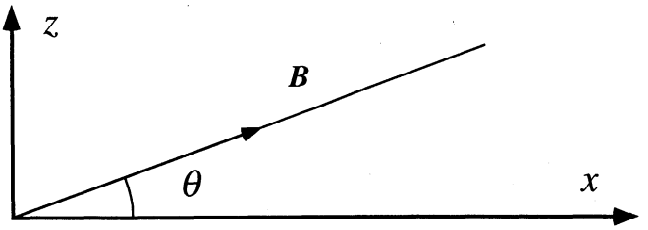

Figure 1. The equilibrium model has a uniform magnetic field $\mathbf{B} = B(\cos\theta, 0, \sin\theta)$, θ being an arbitrary angle. The density ρ depends solely upon z, and consequently, if θ is nonzero ρ changes along a field line.

To date, most studies have concentrated upon one-dimensional tail equilibria in which quantities vary in the z coordinate and the magnetic field is taken to be parallel/antiparallel to x. Within such an idealized model, fast waves which do not propagate across the tail ($k_y = 0$) decouple from the Alfven mode, and these normal modes ($\propto \exp(-i\omega t)$) have received much attention [e.g., *Hopcraft and Smith*, 1986]. A summation of these modes can describe how impulsive fast mode sources, such as substorms, may propagate along the tail waveguide [*Edwin et al.*, 1986; *Berghmans et al.*, 1996]. Indeed, *Edwin et al.* [1986] suggest this may explain the classic Pi2 signature.

If waves are considered for which k_y may be nonzero, the equilibrium described above will generally couple fast and Alfvén waves. *Seboldt* [1990] and *Liu et al.* [1995] both considered solutions with a dependence $\propto \exp i(k_x x + k_y y - \omega t)$ and showed that the well-known Alfvén resonance occurred at a particular value of z for which the Alfvén frequency ($\omega_A(z) = k_x V_A(z)$) matched the normal mode frequency. Formally, this solution is identical to the result established by *Southwood* [1974]. Recently, *Allan and Wright* [1998] have generalized this work to the time-dependent domain by solving the impulsively driven equations numerically. They found that fast and Alfvén waves were still coupled, but an extended layer of field lines (probably in the PSBL) has Alfvén waves excited on it preferentially.

The equilibrium in all of these studies (except for *Hansen and Harrold* [1994], *Schwartz and Bel* [1984] and *Wright and Garman* [1998]) satisfies $(\mathbf{B}\cdot\nabla)\rho = 0$, and the associated linear ordinary differential equation (ODE) of the normal mode is singular and second-order. All these studies showed that if the equilibrium density varied along the background field, as must be the case in the real magnetotail, the resulting normal modes of the governing fourth-order equation were not singular. Hansen and Harrold's [1994] solution had some unusual properties, for example, the time-averaged z component of the Poynting flux was found to be dependent on z. It is essential that this system is understood properly if we are to be able to interpret data relevant to wave coupling in the tail. *Wright and Garman* [1998] reexamined the *Hansen and Harrold* [1994] calculation and noted some fundamental differences between their solution and that of *Hansen and Harrold* [1994]. In particular, the time-averaged z component of the Poynting flux is independent of z, and although efficient coupling of fast and Alfvén waves still occurs at the "resonant" position, the Alfvén waves propagate away from this position, preventing the formation of a singularity.

Although *Wright and Garman* [1998] found evidence of strong wave coupling in the normal modes of the fourth-order equations, even in the limit $(\mathbf{B}\cdot\nabla)\rho \to 0$, their character was completely different from those of the second-order equations associated with the case $(\mathbf{B}\cdot\nabla)\rho = 0$. In the latter case, there is an accumulation of energy at a certain position where the Alfvén wave fields have infinite amplitude. In the former case, there is no accumulation of Alfvén wave energy at any specific position. The calculation we present here is able to show that these two contrasting types of solution are actually different limits of the more general time-dependent solution. We provide quantitative criteria for when the different types of behavior occur, and this enables us to deduce the structure of driven Alfvén waves. Essentially, we find that for early times the evolution is similar to the more familiar resonant coupling which occurs when $(\mathbf{B}\cdot\nabla)\rho = 0$ [e.g., *Mann et al.*, 1995] and Alfvén wave energy accumulates around the coupling (or resonant) position. For large times energy is radiated away, and the solution asymptotes to the nonsingular normal modes found by *Wright and Garman* [1998].

Our main conclusion is that efficient fast and Alfvén wave coupling can occur even when $(\mathbf{B}\cdot\nabla)\rho \neq 0$. Our results indicate that Alfvén waves driven by impulsively generated fast modes within the tail (e.g., reconnection events) may be observed on field lines mapping to the PSBL, and we are able to suggest potential observations that would support our theory. For example, we predict whether these waves propagate toward or away from the Earth and also toward or away from the plasma sheet. It has recently been suggested that negative-energy surface waves on the magnetopause can couple to Alfvén waves in the plasma mantle [*Ruderman and Wright*, 1998], and we make predictions about the propagation features of these waves, too.

The paper is structured as follows: Section 2 describes our model and relevant length scales; section 3 discusses three numerical data sets which demonstrate the different character of possible waves; section 4 discusses the relevance of our results to data and describes potentially observable results; and section 5 summarizes our main conclusions. Details of the numerical scheme and boundary conditions are given in the appendix.

2. Model and Governing Equations

We adopt the simple model suggested by *Hansen and Harrold* [1994] in which a uniform magnetic field is inclined at some angle θ to the $\hat{\mathbf{x}}$ direction; $\mathbf{B} = B(\cos\theta, 0, \sin\theta)$ (see Figure 1). The density is an arbitrary function of $z, \rho(z)$, so $(\mathbf{B}\cdot\nabla)\rho = B\sin\theta d\rho/dz$

is generally nonzero unless θ is identically zero. This model may represent a portion of the northern half of the tail.

Since the equilibrium is invariant in x and y, we may seek solutions of the form

$$f(z,t)\exp i(k_x x + k_y y) \tag{1}$$

Note that $f(z,t)$ is a complex function. Following *Hansen and Harrold* [1994], we neglect plasma pressure and seek solutions to the ideal, linearized MHD equations,

$$\rho\frac{\partial \mathbf{u}}{\partial t} = (\nabla\wedge\mathbf{b})\wedge\mathbf{B}/\mu_0 \tag{2a}$$

$$\frac{\partial \mathbf{b}}{\partial t} = \nabla\wedge(\mathbf{u}\wedge\mathbf{B}) \tag{2b}$$

where $\mathbf{b}$ and $\mathbf{u}$ are the field and flow perturbations. Note that the plasma acceleration is always perpendicular to $\mathbf{B}$, and thus

$$u_x = -u_z\tan\theta \tag{3}$$

Throughout the rest of this paper we shall use dimensionless quantities: Lengths are normalized by the extent ℓ of the domain in z; density is normalized by ρ_0 (the density at either $z = 0$ or 1); magnetic fields are normalized by B; speeds are normalized by $V_0 = B/\sqrt{\mu_0\rho_0}$ (where $V(z) = B/\sqrt{\mu_0\rho(z)}$ is the Alfvén speed); and time is normalized by ℓ/V_0.

Eliminating u_x in favor of u_z using (3), the fields may be written as the state vector

$$\mathbf{U}^T = (b_{xr}, b_{xi}, b_{yr}, b_{yi}, b_{zr}, b_{zi}, u_{yr}, u_{yi}, u_{zr}, u_{zi}) \tag{4}$$

(the superscript T denotes the transpose, and the subscripts r and i denote real and imaginary parts, respectively).

The governing equations (2) take the form

$$\frac{\partial \mathbf{U}}{\partial t} - \mathbf{F}(\mathbf{U}) = 0 \tag{5}$$

The vector $\mathbf{F}$ is defined in terms of the vector $\mathbf{C}$ and matrix $\mathbf{M}$,

$$\mathbf{F} + \mathbf{M}\cdot\frac{\partial \mathbf{U}}{\partial z} + \mathbf{C} = 0 \tag{6}$$

where $\mathbf{M}$ is a 10×10 matrix whose elements (m_{ij}) are zero except for

$$m_{19} = m_{2,10} = \sec\theta \tag{7a}$$

$$m_{37} = m_{48} = -\sin\theta \tag{7b}$$

$$m_{73} = m_{84} = -\sin\theta/\rho \tag{7c}$$

$$m_{91} = m_{10,2} = \cos\theta/\rho \tag{7d}$$

The elements of $\mathbf{C}$ are

$$\mathbf{C} = \begin{pmatrix} -k_y\cos\theta u_{yi} \\ k_y\cos\theta u_{yr} \\ k_x\cos\theta u_{yi} \\ -k_x\cos\theta u_{yr} \\ k_x\sec\theta u_{zi} - k_y\sin\theta u_{yi} \\ -k_x\sec\theta u_{zr} + k_y\sin\theta u_{yr} \\ -(k_y\cos\theta b_{xi} - k_x\cos\theta b_{yi} + k_y\sin\theta b_{zi})/\rho \\ (k_y\cos\theta b_{xr} - k_x\cos\theta b_{yr} + k_y\sin\theta b_{zr})/\rho \\ k_x\cos\theta b_{zi}/\rho \\ -k_x\cos\theta b_{zr}/\rho \end{pmatrix} \tag{8}$$

The motivation for writing $\mathbf{F}$ in terms of $\mathbf{M}$ and $\mathbf{C}$ is that the z derivatives are isolated. This will be useful when updating the equations numerically at the edge of our domain, as centered differences in z may not be employed there. Instead, we will sometimes use a characteristic boundary condition for which the form in (6) is required [*Sun et al.*, 1995].

The solutions we present in this paper demonstrate the importance of two length scales. We shall introduce them here to facilitate a detailed interpretation of the results to follow. The phase mixing length (L_{ph}) is defined to be

$$L_{ph} = \frac{2\pi}{\omega_A' t};\quad \omega_A' = \frac{d\omega_A}{dz} \approx k_x\frac{dV}{dz} \tag{9}$$

where $\omega_A(z)$ is the Alfvén frequency ($\approx k_x V_A$) of the field line at z. This concept makes sense when $\theta = 0$, i.e., a given field line is confined to a single z coordinate. The formula for L_{ph} shows how neighboring field lines drift out of phase with each other as time increases if they have different Alfvén frequencies ($\omega_A' \neq 0$) [e.g., *Mann et al.*, 1995]. L_{ph} is rather like the wavelength in z, i.e., the distance between two peaks in displacement. When $\theta \neq 0$, a single field line maps to all z, if we trace far enough along the field. Thus the idea of each field line having a unique Alfvén frequency that is a function of z does not make sense. However, we shall see that in certain limits the solution is very similar to the $\theta = 0$ case, and it is useful to define $\omega_A(z) \approx k_x V$ when θ is small.

When $\theta \neq 0$, Alfvén waves propagate in the z direction. After a time t the distance propagated in z will be of order

$$L_z = V_z t = Vt\sin\theta \tag{10}$$

(where we have neglected the variation of V with z in this order of magnitude estimate).

We define α to be the ratio of L_z and L_{ph},

$$\alpha = \frac{L_z}{L_{ph}} \approx \frac{Vt^2\sin\theta}{\lambda_x}\cdot\frac{dV}{dz} \tag{11}$$

where $\lambda_x = 2\pi/k_x$. We shall show that when $\alpha \ll 1$ (i.e., $L_z \ll L_{ph}$), the propagation in z is negligible, so we may ignore the tilt of the field and set $\theta = 0$. The

evolution should be similar to the solutions of *Mann et al.* [1995] in this regime.

When $\alpha \sim O(1)$ the distance propagated in z (which is now of order the phase mixing length) may not be neglected, i.e., the tilt of the field is important, and the solution will differ from the $\theta = 0$ case. We define the time t_c to be when $\alpha(t = t_c) = 1$.

If $\alpha \gg 1$, for example, when t is large, the tilt of the field dominates the solution which no longer resembles the $\theta = 0$ solutions. Indeed, for a steadily driven ($\exp(-i\omega t)$) system with $\alpha \gg 1$, we would expect the solutions to asymptote to the $\theta \neq 0$ normal modes described by *Wright and Garman* [1998], in which the time-averaged z component of the Poynting flux is independent of z.

3. Numerical Results

Details of the numerical scheme accuracy and boundary conditions are given in the appendix. We present three sets of results here which focus upon different α regimes. The different runs each have a density and Alfvén speed profile that is suited to demonstrating certain features. The normalized Alfvén speed for each model is shown in Figure 2. The Alfvén speed is uniform for $0 < z < z_1$ and $z_2 < z < 1$, having the values $V(0)$ and $V(1)$, respectively. Over the interval $z_1 < z < z_2$ the Alfvén speed varies according to

$$V(z) = \frac{1}{2}(V(0) + V(1)) - \frac{1}{2}(V(1) - V(0)) \times \cos\left(\pi \frac{z - z_1}{z_2 - z_1}\right) \quad (12)$$

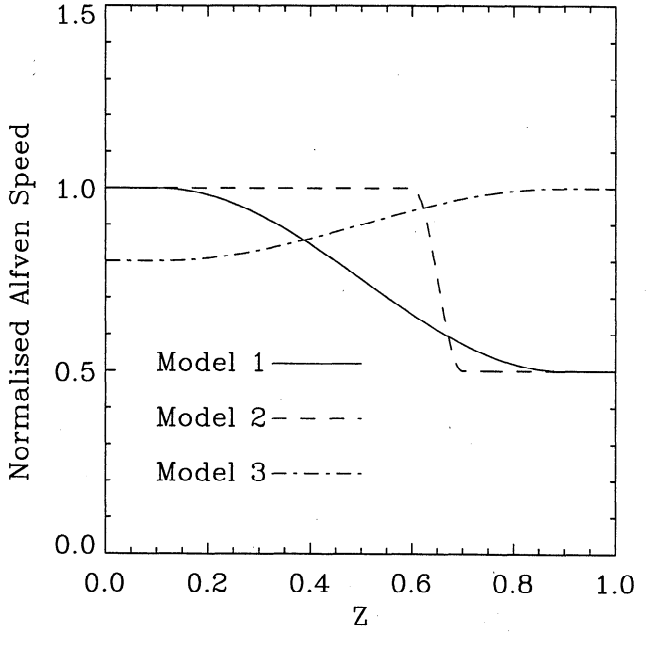

Figure 2. The Alfvén speed profiles for the three models used in this paper. (Analytical forms are described in the text.)

The values of $(z_1, z_2, V(0), V(1))$ are (0.1, 0.9, 1.0, 0.5), (0.6, 0.7, 1.0, 0.5), and (0.1, 0.9, 0.8, 1.0) for models 1, 2, and 3, respectively.

3.1. Run 1: $\alpha \leq 1$

The parameters in this run are chosen to study the early development of wave coupling, and the equilibrium model 1 is used ($k_x = 8.3776, \tau = 1.0, k_y = 1.0$). These parameters are such that if $\theta = 0$, we would expect there to be an Alfvén resonance where $V(z) = 0.75$, i.e., $z = 0.5$. The boundary at $z = 0$ is held as a perfectly reflecting boundary, while the one at $z = 1$ has u_z forced with period τ (see the appendix for details). Figure 3 shows u_{yr} snaphots for the times $t = 2.5, 5.0, 7.5$, and 10.0. The dashed line is the result for $\theta = 0$ with which we contrast the solid line for $\theta = 0.01$. At $t = 2.5$ the amplitude is very small, and u_{yr} has a global structure, as it is associated with the fast mode. At later times, u_{yr} has a larger amplitude and is centred upon $z = 0.5$, where Alfvén waves are expected to be excited. The value of α for the different snapshots is also given. We see that when $\alpha = 0.05$ or 0.25, there is very little difference between the tilted ($\theta = 0.01$, solid line) and untilted ($\theta = 0.0$, dashed line) solution. This demonstrates that when $L_z \ll L_{ph}$, the tilt of the field is unimportant. At later times ($t = 7.5$ and 10.0) the distance propagated in z by the waves is of order the phasemixing length, and the two solutions differ increasingly with time. The Alfvén waves excited around $z = 0.5$ may propagate in z when $\theta = 0.01$, whereas when $\theta = 0.0$ the Alfvén waves must stay near $z = 0.5$. This property manifests itself as the dashed line having a larger amplitude than the solid line near $z = 0.5$.

3.2. Run 2: $1 < \alpha < 16$

Run 2 is designed to study the medium-term evolution of the waves and employs the Alfvén speed in model 2. The dashed lines in Figure 4 at $z = 0.6$ and 0.7 delineate the two regions $0 < z < 0.6$ and $0.7 < z < 1.0$, which contain a uniform medium in which there will be no wave coupling of fast and Alfvén modes. The nonuniform section $0.6 < z < 0.7$ is where any mode coupling will occur.

The parameters used in run 2 are $k_x = 16.755, \tau = 0.5, k_y = 1.0, \theta = 0.08$, and Figure 4 summarizes the results taken up to the time $t = 8.0$, when $\alpha = 16.0$. This large value of α means that the propagation of Alfvén waves away from the coupling site should be an important feature of the solution. On the basis of the results of *Wright and Garman* [1998] we expect strong coupling to occur at $z = 0.65$, where $2\pi/\tau = k_x V$. The duration of the run is sufficiently short that Alfvén waves will not reach the ends of the domain, so we employ the reflecting boundary condition at $z = 0$ and the driven one at $z = 1.0$.

The top panel of Figure 4 shows the structure of the fast mode at $t = 8.0$: u_{zr} and b_{xr} have an oscillatory

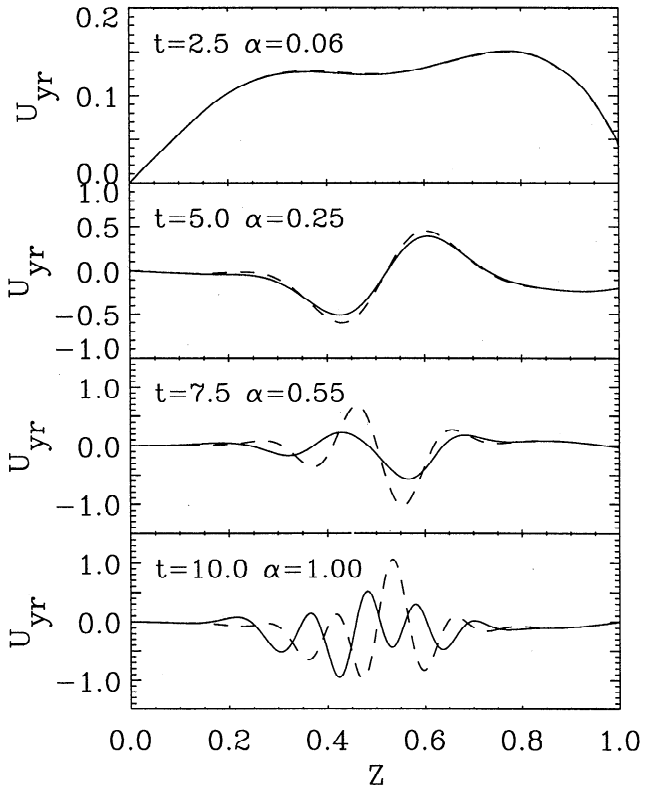

Figure 3. Snapshots of u_{yr} for run 1. The dashed lines correspond to $\theta = 0.0$, and the solid lines correspond to $\theta = 0.01$. Other parameters are given in the text.

spatial variation for $z > 0.7$ and an approximately exponential decay for $z < 0.6$. The presence of a turning point at $z \approx 0.65$ is also evident. The lower three panels show the Alfvén wave fields. At $t = 2.0$ ($\alpha = 1.0$) the waves are concentrated in $0.6 < z < 0.7$, where mode coupling is expected to occur. When $t = 4.0$ ($\alpha = 4.0$), Alfvén waves are propagating into the two uniform regions $z < 0.6$ (b_{yr} and u_{yr} in phase) and $z > 0.7$ (b_{yr} and u_{yr} out of phase). For Alfvén waves we expect $u_y/V = \pm b_y/B$, where the plus and minus signs correspond to propagation antiparallel and parallel, respectively, to **B** (since θ is positive, **B** is directed from $z = 0$ to $z = 1$.). Thus, in normalized units, we expect $u_{yr} = +b_{yr}(z < 0.6)$ and $u_{yr} = -0.5b_{yr}(z > 0.7)$, in agreement with Figure 4.

The bottom panel of Figure 4 shows a clear wavelength in z emerging for the Alfvén waves when $t = 8.0$ ($\alpha = 16.0$). *Wright and Garman* [1998] give an expression for this wavelength

$$\lambda_z(z) = \frac{2\pi}{k_z} = \frac{2\pi}{k_x} \cdot \frac{\sin\theta}{V(z_c)/V(z) - \cos\theta} \qquad (13)$$

where $V(z_c) = \omega/k_x \cos\theta$. They also show that for small θ the position z_c and the quasi-resonant position z_r (where $2\pi/\tau = k_x V(z_r)$) are virtually identical; $z_c = z_r + O(\theta^2)$. (Note that we have allowed for the Alfvén waves in $z < 0.6$ propagating to $x = -\infty$, while those in $z > 0.7$ propagate to $x = +\infty$, when adapting Wright and Garman's result; see later.) Equation (13) predicts the wavelengths $\lambda_z(z < 0.6) = 0.12$ and $\lambda_z(z > 0.7) = 0.06$, which are plotted as horizontal lines in the bottom panel of Figure 4. These lengths agree extremely well with the peak-to-peak spacing in u_{yr}.

It is interesting that the coupling region generates Alfvén waves propagating in both directions; this is different from the normal modes derived by *Wright and Garman* [1998] that only propagated to larger z (particularly clear in their Figure 5). The reason is that Wright and Garman's modes can be thought of as being driven by the u_z condition at $z = 1$ of $u_z(z = 1) \exp i(k_x x - \omega t)$ for a suitable time origin. Taking the real part gives $\cos(k_x x - \omega t)$, which corresponds to propagation in the positive x direction. The solutions presented here are generated by a boundary condition at ($z = 1$) of the form $u_z(z = 1, t) \exp i(k_x x)$. Taking the real part yields terms of the form $u_{zr}(1, t) \cos(k_x x)$ (see section A4 for more details), which do not have phase propagation in x, but stand. This can be seen by driving the boundary at a single frequency, so the x and t dependence of the physical z component of the velocity at $z = 1$

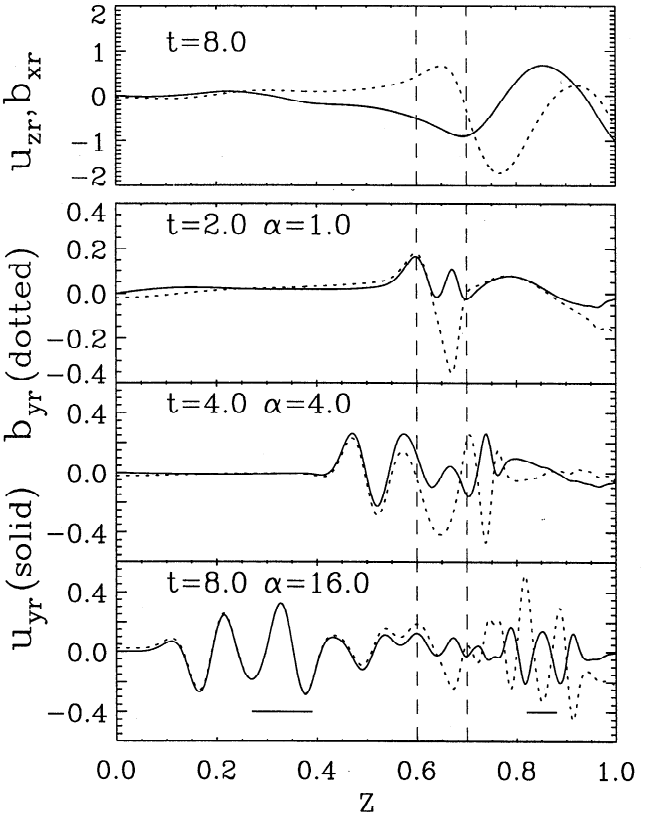

Figure 4. The top panel shows a snapshot of the fast mode fields u_{zr} (solid line) and b_{xr} (dotted line). The bottom three panels show successive snapshots of the Alfvén wave fields u_{yr} (solid lines) and b_{yr} (dotted lines). The parameters for this run (run 2) are given in the text.

is $\cos(\omega t)\cos(k_x x)$. We can, of course, consider this standing wave as a superposition of traveling waves,

$$2\cos(\omega t)\cos(k_x x) = \cos(k_x x - \omega t) + \cos(k_x x + \omega t) \quad (14)$$

The *Wright and Garman* [1998] solution only has terms like the first one on the right-hand-side of (14). By superposing two Wright and Garman modes (one with k_x positive, the other with k_x negative) we would get solutions that radiated waves in both z directions from the coupling site, like the results in Figure 4. Indeed, when calculating the wavelength in (13) we had to allow for a change of sign of k_x for the waves in $0 < z < 0.6$ when adapting the Wright and Garman formula.

The Alfvén waves propagating in each direction in Figure 4 carry a time-averaged (over one cycle) normalized Poynting flux in the z direction of $\langle S_z \rangle = B_z(u_{yr}b_{yr} + u_{yi}b_{yi})/2$ which is actually equal and opposite for the two groups of waves. (This result was established quantitatively in other results that are not shown here.)

3.3. Run 3: $\alpha \gg 1$

Run 3 is designed to study the long-term behavior of the waves and confirms that the results can asymptote to a normal mode, for which $\langle S_z \rangle$ should be independent of z. The parameters used in this run (which used the Alfvén speed variation of model 3) are $k_x = 6.6139, k_y = 1.0, \tau = 1.0$, and $\theta = 0.2$. The simulation is run up to a time of 25.0, during which time the Alfvén waves will have propagated to the boundaries at $z = 0.0$ and 1.0.

In order to allow the system to asymptote to a "normal mode," where all quantities vary as $\exp(-i\omega t)$, it is necessary to drive the system but also to allow any Alfvén waves that reach the boundaries to propagate out of the domain $0 < z < 1$, rather than be reflected and trapped. This is accomplished easily enough at $z = 0$, where the outgoing boundary condition is employed. The boundary at $z = 1.0$ is more awkward, since we wish to drive a fast wave here, but also allow Alfvén waves to propagate out of the simulation domain: The driven/leaky boundary condition described in section A4 produces this type of behavior and was imposed at $z = 1.0$.

The dependence of $\langle S_z \rangle$ on z for four time intervals is shown in Figure 5. $\langle S_z \rangle$ is always negative and represents the net transport of energy from the driven boundary ($z = 1.0$) in the negative $\hat{\mathbf{z}}$ direction to the leaky boundary ($z = 0.0$). For $0 < t < 1.0$, $\langle S_z \rangle$ is zero for $0 < z < 0.2$, as the waves launched from $z = 1.0$ have not reached there yet. At a later time ($1 < t < 2$, dotted line), energy is leaking out of the $z = 0$ boundary but not as quickly as it is being supplied at $z = 1.0$. As early as $2 < t < 3$ (dashed line), $\langle S_z \rangle$ is showing indications of becoming independent of z, and at a much later time ($24 < t < 25$, dash-dotted line) $\langle S_z \rangle$ is essentially constant. Indeed, $\alpha(t = 25) \approx 50$ for this run, suggesting the solution should look more like a normal mode than a ($\theta = 0$) growing resonance. The fact that $\langle S_z \rangle$ is independent of z rather than having a "jump" across the ($\theta = 0$) resonant position confirms this interpretation.

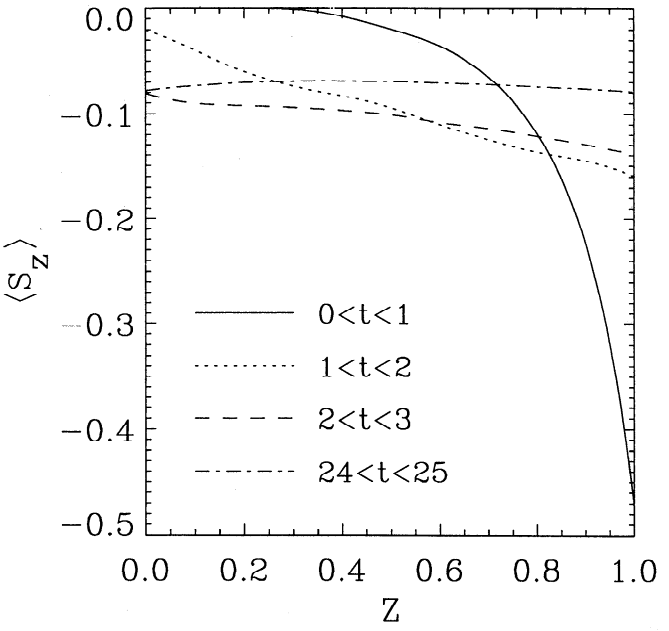

Figure 5. Plots of the time-averaged z component of the Poynting flux $\langle S_z \rangle$ for run 3. The curves show $\langle S_z \rangle$ at different times. As time increases, $\langle S_z \rangle$ becomes increasingly independent of z.

4. Observations

In this section we address the implications of our results for wave behavior in the tail and describe the signatures likely to be seen in ground-based and satellite data sets. Figure 6 shows a diagram of the magnetotail. In the center of the plasma sheet is a region that radiates fast waves (e.g., a reconnection event). *Allan and Wright* [1998] show that on the sunward/antisunward side of the source there only exist fast waves propagating in the sunward/antisunward direction. Of course, a general fast mode disturbance may be thought of as a summation of propagating k_x Fourier modes. *Allan and Wright*'s [1998] detailed solutions (in the $\alpha < 1$ regime) show how the resonant wave coupling at a given z is dominated by a single k_x mode and is thus similar to the model presented here. The numerical solutions we considered had a standing structure which corresponded to the combination of two solutions propagating in the sunward and antisunward directions. Evidently, we need only consider each component in isolation for this particular situation.

In the northern PSBL we expect Alfvén wave propagation to be parallel/antiparallel to **B** for observa-

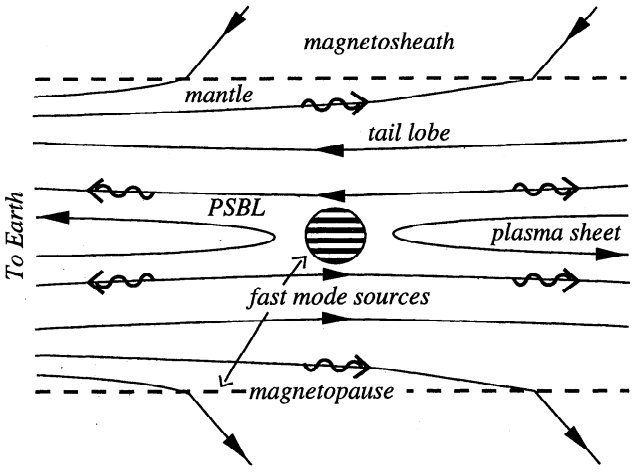

Figure 6. A sketch of the magnetotail field in the (x, z) plane. Fast waves may originate from the center of the tail from reconnection events and substorms or from the magnetosheath flow, which may excite a negative-energy fast surface wave on the magnetopause. These waves may couple to Alfvén waves (denoted by the rippled arrows) in the plasma sheet boundary layer or the plasma mantle. The direction of propagation of the Alfvén waves is shown in these regions.

tions on the sunward/antisunward side of the fast mode source region. In the southern PSBL we expect Alfvén wave propagation to be parallel/antiparallel to **B** for observations on the antisunward/sunward side of the fast mode source region. Hence a positive identification of a propagating Alfvén wave in the PSBL is sufficient to constrain the location of the observing spacecraft relative to the fast mode source region. Once the earthward traveling PSBL Alfvén waves reach the ionosphere and suffer significant reflection, the structure of the waves will be composed of an incident and reflected Alfvén wave which will locally look like a standing wave if the waveform is observed after the initial wave front has reached the ionosphere, which is the most likely case. Thus low-altitude satellites may see a standing Alfvén wave signature, whereas satellites in the deep tail will see propagating wave signatures. Unfortunately, published ULF wave observations from low-altitude spacecraft have generally concentrated on dayside events [e.g., *Potemra and Blomberg,* 1996]. There is little available information on the behavior of potential PSBL waves at low altitudes.

It has recently been suggested that negative-energy surface waves on the tail's magnetopause can exist whenever the sheath flow speed has a magnitude between the sheath sound speed and tail lobe Alfvén speed [*Ruderman and Wright,* 1998]. (If the flow speed exceeds the Alfvén speed, the boundary suffers from the Kelvin-Helmholtz instability.) These authors show how the negative-energy wave must propagate antisunward, and also that it may drive Alfvén waves in the nonuniform plasma mantle. If there are no field lines passing through the tail magnetopause ($\mathbf{B} = B\hat{\mathbf{x}}$) then the analysis of Ruderman and Wright is appropriate. However, if field lines pass through the magnetopause so that the mantle field is tilted, as shown in Figures 1 and 6, then the behavior described in the present paper is applicable. Mantle Alfvén waves driven by magnetopause waves should have strictly antisunward propagation (i.e., antiparallel/parallel to **B** in the northern/southern mantles). Consequently, the propagation is always toward the magnetopause where the waves may suffer partial transmission to the magnetosheath or partial reflection back into the tail.

Whether the wave coupling occurs in the small or large α limit requires a knowledge of the equilibrium Alfvén speed variation, orientation of the field, the period of the waves (τ), and the number of cycles of Alfvén waves excited (N). These quantities would have to be estimated from a carefully analyzed set of observations, but once they have been determined the following formula may be employed (based upon equation (11))

$$\alpha = N^2 \sin(\theta) \tau \frac{dV}{dz} \tag{15}$$

Here we have taken the evolution time of the system to be $t = N\tau$, a conservative minimum elapsed time for the observed event. Taking the PSBL parameters used by *A. Wright et al.* (submitted manuscript, 1998) as typical, we have $\tau = 670$ s and $dV/dz \approx 100\ \mathrm{km s^{-1}}\ R_E^{-1}$. By estimating the number of cycles of waves in their data we may use (15) to calculate the value of θ for which $\alpha = 1$. Their data show about six cycles, but we shall again be conservative and assume there were only three coherent oscillations, as the entire event may not have been a single wave packet. These values indicate that to make $\alpha < 1$ the background field would have to have been aligned with the density contours to within 0.5°. Otherwise, α exceeds 1, and the tilt of the field is significant. It seems extremely likely that the physical tail equilibrium does not satisfy this stringent criterion, and we conclude that wave coupling almost certainly does not occur in the $(\mathbf{B} \cdot \nabla)\rho = 0$ limit that most previous studies have focused upon. However, we must bear in mind that the simulation we have described here considers only a single Fourier component in x. Recent two-dimensional time-dependent simulations in a model magnetotail [*Allan and Wright,* 1998] have shown that the summation of such modes required to give the full two-dimensional structure can result in quite different behavior to a single Fourier mode. Therefore a true two-dimensional simulation of the present system would be of considerable interest.

5. Summary

Our time-dependent simulations have demonstrated that the configuration shown in Figure 1 can permit efficient coupling between fast and Alfvén waves even when $\theta \neq 0$. For $\alpha \ll 1$ (satisfied when θ is suffi-

ciently small) the solution is effectively the same as the $\theta = 0$ case, and the fast energy flux coupled to Alfvén waves will be independent of θ (run 1). As time (and α) increases the Alfvén waves propagate away from the coupling site (run 2) and may asymptote to a normal mode (run 3) in which the time-averaged Poynting flux of the Alfvén waves and the fast wave energy flux coupled to the Alfvén waves must balance. The Alfvén wave Poynting flux has a z component proportional to $B \sin\theta(u_{yr}b_{yr} + u_{yi}b_{yi})$, and for small θ this must be a constant. We can now see how to recover the $\theta = 0$ singularity for a steadily driven system: As $\theta \to 0$, the constancy of Alfvén wave Poynting flux means that u_y and $b_y \to \infty$. Morcover, the distance in z propagated by the Alfvén waves is $L_z = Vt \sin\theta \to 0$ as $\theta \to 0$. Thus the Alfvén waves have an infinite amplitude over an infinitesimal region, i.e., we have a singularity which is familiar from the second-order $\theta = 0$ normal mode equations [*Southwood*, 1974]. Explicitly, the amplitude of the Alfven waves is proportional to $1/\sqrt{\theta}$, and the width in z is proportional to θ (once $L_z > L_{ph}$).

A realistic model of wave coupling in the geomagnetic tail must allow for the fact that the fields are not periodic in x but have a finite extent in x as well as in time. This will result in Alfvén wave packets being excited (rather than the Alfvén wave trains of the present simulations), which will then be guided along the background field. The Alfvén waves arriving at Earth are likely to be more easily observed than fast waves (especially those originating from the distant tail) whose propagation is more isotropic, which results in attenuation.

Appendix

The numerical method used to update the state vector (5) is the leapfrog-trapezoidal scheme [*Zalesak*, 1979]. Given the state vector ($\mathbf{U}$) at two times (t and $t - \Delta t$), we apply the following algorithm to calculate $\mathbf{U}^{t+\Delta t}$:

$$\mathbf{U}^{\dagger} = \mathbf{U}^{t-\Delta t} + 2\Delta t \mathbf{F}^{t} \tag{16a}$$

$$\mathbf{F}^{*} = \frac{1}{2}(\mathbf{F}^{t} + \mathbf{F}^{\dagger}) \tag{16b}$$

$$\mathbf{U}^{t+\Delta t} = \mathbf{U}^{t} + \Delta t \mathbf{F}^{*} \tag{16c}$$

$\mathbf{U}^{\dagger}$ is a prediction for $\mathbf{U}^{t+\Delta t}$ based upon $\mathbf{U}^{t-\Delta t}$ and $\mathbf{F}^{t} \equiv \mathbf{F}(\mathbf{U}^{t})$. $\mathbf{F}^{\dagger} \equiv \mathbf{F}(\mathbf{U}^{\dagger})$ is thus an estimate of $(\partial \mathbf{U}/\partial t)^{t+\Delta t}$, so $\mathbf{F}^{*}$ gives $(\partial \mathbf{U}/\partial t)^{t+\Delta t/2}$. Finally, we take a centered time integration to find a better estimate of $\mathbf{U}^{t+\Delta t}$. The fact that all time integrations are centered means the scheme is second-order accurate in time. The z derivatives required to calculate $\mathbf{F}$ in (6) are also taken as centered differences, so the scheme is second-order accurate in space also. Convergence tests were performed and conservation of energy and $\nabla \cdot \mathbf{b}$ checked. When choosing the number of grid points (n), it is important to ensure that L_{ph} and λ_z (the wavelength in z; see *Wright and Garman* [1998]) are well resolved (typically, $\Delta z \leq \min(L_{ph}, \lambda_z^{\pm})/10$, the plus-minus sign corresponding to the waves propagating parallel and antiparallel to $\mathbf{B}$). The time step (dt) is then chosen according to $dt \ll \Delta z/V$.

To estimate the numerical error, we calculated the magnetic and velocity fields at a specific position (z_0) and time (t_0), normally the finishing time of the simulation. The resulting values will depend upon the spatial resolution (Δz) and the time step (Δt); $f(z_0, t_0, \Delta z, \Delta t)$, where f is a component of $\mathbf{b}$ or $\mathbf{u}$. The simulation was then repeated at a higher resolution ($\Delta z/2, \Delta t/2$) to determine $f(z_0, t_0, \Delta z/2, \Delta t/2)$. The resolution was increased until the resolution had converged to an acceptable error. The relative error (ϵ) in the fields is estimated from

$$\epsilon = \frac{f(z_0, t_0, \Delta z, \Delta t) - f(z_0, t_0, \Delta z/2, \Delta t/2)}{|f(t_0, \Delta z/2, \Delta t/2)|} \tag{17}$$

where the denominator represents the typical magnitude of f over the z domain at $t = t_0$. Below we give details of the numerical error of the wave fields determined by this criterion, the spatial and temporal resolutions employed, and the results of checking the degree to which invariant quantities of our governing equations were conserved at the end of the run time:

In run 1, $n = 1000$ and $dt = 5 \times 10^{-5}$. Wave fields are determined to 0.05%, energy conservation is met to 0.01%, and $\nabla \cdot \mathbf{b} = 10^{-11}$.

In run 2, $n = 2000$ and $dt = 2.5 \times 10^{-5}$. Wave fields are determined to 0.05%, energy conservation is met to 0.02%, and $\nabla \cdot \mathbf{b} = 2 \times 10^{-10}$.

In run 3, $n = 400$ and $dt = 1.25 \times 10^{-4}$. Wave fields are determined to 0.03%, energy conservation is met to 0.03%, and $\nabla \cdot \mathbf{b} = 5 \times 10^{-11}$.

Of course, centered differences are not possible at the ends of the spatial domain, and below we give details of the variety of boundary conditions that were employed in the the three numerical experiments described in this paper. Generally, the boundary conditions were chosen for numerical convenience or to elucidate a certain type of behavior in our preliminary studies. However, these boundary conditions may also be a reasonable first approximation to representing various boundaries in the magnetotail, and we discuss this below. Our one-dimensional model does not permit a realistic inclusion of the ionospheric ends of the field lines. Thus our results are applicable to the evolution of waves in the tail before they encounter the ionosphere.

A1. Reflecting Boundary Condition

At $z = 0$ we frequently impose a perfectly reflecting boundary condition which has $\langle S_z(0) \rangle = 0$. A consistent choice has nodes of $u_{xr}, u_{yr}, u_{zr}, b_{xi}, b_{yi}$, and b_{zi} and antinodes (i.e., $d/dz = 0$) of $u_{xi}, u_{yi}, u_{zi}, b_{xr}, b_{yr}$, and b_{zr}. In practice, this is done by introducing a ghost cell at $z = -\Delta z$, and when calculating $\mathbf{U}^{\dagger}$ and $\mathbf{U}^{t+\Delta t}$ for this cell a simple symmetry or antisymmetry about $z = 0$ is exploited. For example, the elements

u_{xr} and u_{xi} are defined as $u_{xr}(-\triangle z) = -u_{xr}(+\triangle z)$, and $u_{xi}(-\triangle z) = u_{xi}(+\triangle z)$, etc. A reflecting symmetry boundary condition would be a good representation of the center of the plasma sheet (PS) when the tail is driven symmetrically from the northern and southern lobes.

A2. Outgoing Boundary Conditions

An outgoing boundary condition employs the characteristics solution of *Sun et al.* [1995]. The z derivatives at the boundary are calculated using one-sided-derivatives, and no ghost cells are required. The eigenvalues and eigenvectors of the matrix $\mathbf{M}$ in (6) are calculated. The eigenvalues correspond to the group velocity (in z) of different wave modes and the eigenvectors to the perturbations of these waves. The quantity $\mathbf{M} \cdot \partial \mathbf{U}/\partial z$ may be decomposed into a superposition of the different wave modes. For an "outgoing" boundary condition we set the amplitude of any modes with a group velocity into our simulation domain to be zero. Thus $\mathbf{F}$ is calculated based upon waves propagating out of our simulation domain, and the solution loses energy through this boundary.

This boundary condition was chosen for numerical reasons so that we could study how waves are radiated from the coupling site. (Waves returning from the boundaries would cloud this picture.) The outgoing boundary condition could represent the PS/PSBL interface when the duration of the simulation is less than the transit time across the PS. In this limit, waves would propagate into the PS but would not return from it.

A3. Driven Boundary Condition

The driven boundary condition updated $\mathbf{U}$ according to (5) and (6) by using one-sided derivatives at the boundary and no decomposition in terms of characteristics. The equations are driven by prescribing some variables as a function of time on the boundary and simply overwriting these values to the appropriate elements of $\mathbf{U}^{\dagger}$ and $\mathbf{U}^{t+\triangle t}$. (See *Wright and Rickard* [1995] for more details.)

The driven condition we employed on the boundary was

$$u_{zr} = u_{zi} = \begin{cases} \frac{1}{4}\left(1 - \cos\left(2\pi t/\tau\right)\right)^2 & 0 < t < \tau/2 \\ \cos\left(2\pi t/\tau - \pi\right) & t > \tau/2 \end{cases} \tag{18}$$

where the period τ may be chosen. The velocity over the first half cycle is chosen such that u_z and its derivative are continuous at $t = 0$ and $\tau/2$. Only u_z is driven. The other elements of $\mathbf{U}$ are updated on the boundary using (5) and one-sided derivatives. This driving condition could represent the motion of the magnetopause resulting from a strong magnetosheath flow.

Taking the real part of $u_z(z = 1, t) \exp ik_x x$ to correspond to the physical displacement of the boundary yields $u_{zr}\cos(k_x x) - u_{zi}\sin(k_x x) \equiv u_{zr}(\cos(k_x x) - \sin(k_x x))$, since $u_{zr} = u_{zi}$ on the boundary. A little manipulation renders this in the form $-\sqrt{2}u_{zr}(z = 1, t)\cos(k_x x - \pi/4)$ which, after a shift in x and t origin, clearly has the standing wave structure in x described in and around equation (14).

Note that the algorithm in equation (16) requires the state vector to be known at two consecutive time steps. If we always choose to drive the system from an unperturbed state at $t = 0$, we may simply set $\mathbf{U}^{-\triangle t} = \mathbf{U}^0 = \mathbf{0}$ at the first two time levels, so long as this is consistent with the driving condition in equation (18).

A4. Driven/Leaky Boundary Conditions

When driving the system for a long period of time (so that the solution should asymptote to a normal mode), it is inevitable that some Alfvén waves will reach the driving boundary. The driving condition described in the previous subsection actually reflects any fast waves that are incident upon it [*Wright and Rickard,* 1995], and this is appropriate for certain magnetosheath flow speeds [*Mann et al.*, 1998]. If we wish to asymptote to a normal mode, it is necessary to lose some energy and transients through the boundary. We achieve this by imposing an outgoing characteristic update on the Alfvén fields b_y and u_y, while we reflect any fast wave that is incident upon the driven boundary. The latter is implemented by first introducing an incoming fast characteristic wave of equal amplitude to the outgoing fast wave, which has the effect of reflecting any fast mode incident upon the boundary. (Note that the fast characteristic eigenvector contains nonzero b_x and u_z elements.) Second, the driving condition in equation (18) is added to the resulting fields to provide a driven wave component as well.

Although our main concern in devising these boundary conditions was numerical convenience and stability, it is reasonable to expect the fast and Alfvén waves to have different reflection and transmission properties. The driven/leaky boundary condition could be a good model of the magnetopause which is reflective to fast waves but transmissive to Alfvén waves.

Acknowledgments. A.N.W. is supported by a PPARC Advanced Fellowship and is grateful to PPARC and NIWA for funding his visit to the National Institute of Water and Atmospheric Research where this work was performed. W.A. acknowledges support by the New Zealand Foundation for Research, Science and Technology (FRST) through contract C01627.

The editor thanks William Liu and another referee for their assistance in evaluating this paper.

References

Allan, W., and A. N. Wright, Hydromagnetic wave propagation and coupling in a magnetotail waveguide, *J. Geophys. Res., 103,* 2359, 1998.

Berghmans, D., P. De Bruyne, and M. Goossens, The footpoint-driven coronal sausage wave, *Astrophys. J., 472,* 398, 1996.

Edwin, P. M., B. Roberts, and W. J. Hughes, Dispersive ducting of MHD waves in the plasma sheet: A source of Pi2 wave bursts, *Geophys. Res. Lett.*, *13*, 373–376, 1986.

Elphinstone, R. D., et al., The double oval UV auroral distribution, 2, The most poleward arc system and the dynamics of the magnetotail, *J. Geophys. Res.*, *100*, 12,093, 1995.

Hansen, P. J., and B. G. Harrold, Parallel inhomogeneity and the Alfvén resonance, 1, Open field lines, *J. Geophys. Res.*, *99*, 2429, 1994.

Hopcraft, K. I., and P. R. Smith, Magnetohydrodynamic waves in a neutral sheet, *Planet. Space Sci.*, *34*, 1253, 1986.

Liu, W. W., B.-L. Xu, J. C. Samson, and G. Rostoker, Theory and observations of auroral substorms: A magnetohydrodynamic approach, *J. Geophys. Res.*, *100*, 79, 1995.

Mann, I. R., A. N. Wright, and P. S. Cally, Coupling of magnetospheric cavity modes to field line resonances: A study of resonance widths, *J. Geophys. Res.*, *100*, 19,441, 1995.

Mann, I. R., A. N. Wright, and K. Mills, and V. M. Nakariakov, Exitation of magnetospheric waveguide modes by magnetosheath flows, *J. Geophys. Res.*, (in press), 1998.

Potemra, T. A., and L. G. Blomberg, A survey of Pc 5 pulsations in the dayside high-latitude regions observed by Viking, *J. Geophys. Res.*, *101*, 24,801, 1996.

Ruderman, M., and A. N. Wright, Excitation of Alfvén waves in the magnetosphere by negative-energy surface waves on the magnetopause, *J. Geophys. Res.*, (in press), 1998.

Samson, J. C., D. D. Wallis, T. J. Hughes, F. Creutzberg, J. M. Ruohoniemi, and R. A. Greenwald, Substorm intensifications and field line resonances in the nightside magnetosphere, *J. Geophys. Res.*, *97*, 8495, 1992.

Schwartz, S. J., and N. Bel, On the absence of critical levels in the solar atmosphere, *Solar Phys.*,, *92*, 133, 1984.

Seboldt, W., Nonlocal analysis of low-frequency waves in the plasma sheet, *J. Geophys. Res.*, *95*, 10,471, 1990.

Southwood, D. J., Some features of field line resonances in the magnetosphere, *Planet. Space Sci.*, *22*, 483, 1974.

Sun, M. T., S. T. Wu, and M. Dryer, On the time-dependent numerical boundary conditions of magnetohydrodynamic flows, *J. Comput. Phys.*, *116*, 330, 1995.

Walker, A. D. M., J. M. Ruohoniemi, K. B. Baker, R. A. Greenwald, and J. C. Samson, Spatial and temporal behavior of ULF pulsations observed by the Goose Bay HF radar, *J. Geophys. Res.*, *97*, 12187, 1992.

Wright, A. N., and A. R. Garman, MHD wave coupling in the geomagnetic tail with field-aligned density variations, *J. Geophys. Res.*, *103*, 2377, 1998.

Wright, A. N., and G. J. Rickard, A numerical study of resonant absorption in a magnetohydrodynamic cavity driven by a broadband spectrum, *Astrophys. J.*, *444*, 458, 1995.

Zalesak, S. T., Fully multidimensional FCT algorithms for fluids, *J. Comput. Phys.*, *31*, 335, 1979.

Ziesolleck, C. W. S., and D. R. McDiarmid, Auroral latitude Pc 5 field line resonances: Quantized frequencies, spatial characteristics, and diurnal variation, *J. Geophys. Res.*, *99*, 5817, 1994.

W. Allan, National Institute of Water and Atmospheric Research, P. O. Box 14-901, Kilbirnie, Wellington, New Zealand. (e-mail: w.allan@niwa.cri.nz)

Andrew N. Wright, Mathematical Institute, University of St. Andrews, Fife KY16 9SS, Scotland. (e-mail: andy@dcs.st-and.ac.uk)

(Received February 6, 1998; revised May 8, 1998; accepted June 8, 1998.)